Applied Thermal Engineering 140 (2018) 208–216

Contents lists available at ScienceDirect

Applied Thermal Engineering

journal homepage: www.elsevier.com/locate/apthermeng

Research Paper

Development and numerical modelling of a supercharging technique for positive displacement expanders

Fabio Fatigati[a], Giuseppe Bianchi[b,*], Roberto Cipollone[a]

[a] University of L'Aquila, Department of Industrial and Information Engineering and Economics, L'Aquila 67100, Italy
[b] Brunel University London, Institute of Energy Futures, Center for Sustainable Energy Use in Food Chains, Uxbridge, Middlesex UB8 3PH, UK

HIGHLIGHTS

- Injecting hot fluid during the expansion raises the cell pressure and increases the power output.
- Implementation in a validated numerical model of a sliding vane ORC expander is carried out.
- Effects of the supercharging on the angular pressure evolution are emphasized.
- Benefits in the additional mechanical power output range from 43% to 70%.

GRAPHICAL ABSTRACT

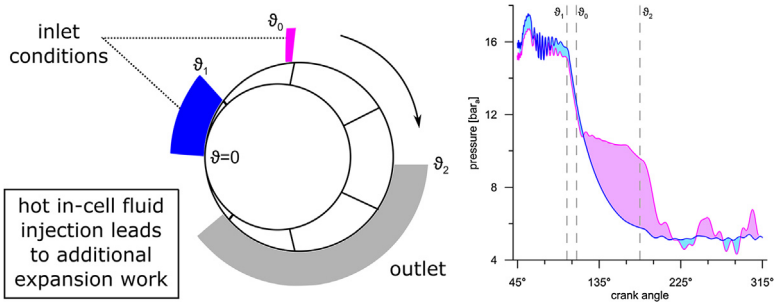

ARTICLE INFO

Keywords:
Waste heat recovery
Organic Rankine Cycle
Automotive
Internal combustion engine
Positive displacement expander
Sliding vane expander

ABSTRACT

This study presents a novel strategy to enhance the recovery performance of any positive displacement expander technology which aims at the maximization of the power output rather than solely its efficiency. The approach is based on an auxiliary injection of fluid under the same suction conditions as the main intake but during the closed volume expansion phase. The operating principle of the supercharging technology is firstly outlined in theoretical terms, while the benefits over a conventional configuration are numerically assessed with reference to a sliding vane expander for applications based on Organic Rankine Cycles (ORC). The holistic modelling platform used for the benchmarking is preliminarily validated over an experimental campaign in which the vane expander was installed in a heavy-duty automotive ORC system and generated up to 1.9 kW (3% of the engine mechanical power) with an overall efficiency of 51.2%. After the simulation platform is validated, the auxiliary intake line is parameterized in terms of four geometrical quantities and the effects of the supercharging with respect to baseline angular pressure trace are shown. An optimization based on a genetic algorithm is eventually performed and the resulting optimized design led to an average mechanical power increase of 50.6%.

1. Introduction

The need for lowering the environmental impact of transportation is of paramount importance and nowadays it is a concern of global exposure. In this context, the interest shown in the development of automotive heat to power conversion systems based on Organic Rankine Cycles (ORC) is proven by the growing number of papers and patents in this area [1,2]. Current research projects in the engine ORC field mostly focus on small-scale systems since in large scale applications, such as the internal combustion engines (ICE) in marine bunkers or gensets, ORC power units already have a mature technology readiness level [3].

The ORC technology can benefit from knowledge and equipment

* Corresponding author.
E-mail address: giuseppe.bianchi@brunel.ac.uk (G. Bianchi).

https://doi.org/10.1016/j.applthermaleng.2018.05.046
Received 6 February 2018; Received in revised form 17 April 2018; Accepted 10 May 2018
Available online 11 May 2018

Nomenclature

p	pressure [Pa]
w	weighting coefficient
D	diameter [m]
L	length [m]
V	volume [m^3]
W	work [J]
Y	dependent variable
ϑ	crank angle [°]
η	efficiency

Subscripts

0	auxiliary suction start
1	primary suction end
2	closed volume expansion end

already developed in sectors like the refrigeration one. However, an automotive application involves additional challenges that do not apply in stationary ORC-based energy recovery systems, such as weight, system integration and energy flow management [4]. In fact, the weight of the ORC system, which also depends on the plant layout complexity, is a parameter that not only affects the overall cost of the energy recovery unit but also the net overall benefits achievable [5]. In this regard, an industrial rule of thumb states that an additional weight of 100lbs decreases the fuel economy by approximately 1%. Moreover, the integration of the ORC equipment with the engine and vehicle architectures involves design challenges from different perspectives: positioning of components, effects on the engine operation (e.g. evaporator back-pressure [6]), control of the ICE + ORC super-system [7]. Finally yet importantly, the introduction of a heat to power conversion unit highly changes the overall engine and vehicle energy balance. For instance, more thermal power is dissipated at low temperatures since the heat rejection related to the engine cooling and lubrication circuits is increased by the heat duty of the ORC condenser. Furthermore, the input power for the pressurization of the working fluid has to be provided by the engine either in mechanical or electrical form; similarly for the output power delivered from the expander to the engine [8].

All these considerations affect the selection and the design of the expansion technology for an automotive ORC system. The amount of literature in this topic is continuously increasing and a comprehensive bibliographic survey is beyond the scope of the current research work. Nevertheless, it is worth to mention that automotive ORC expanders are usually differentiated for their operating principle, namely turbo (radial or axial) or positive displacement expanders (scroll, piston, swash-plate, gerotor, single and twin screw etc.) [9,10]. Compared to other positive displacement technologies, sliding vane machines are analyzed to a limited extent in the literature as well as in terms of industrial market share. For instance, out of 100 new compressors sold worldwide only the 20% is not a screw compressor [11]. The first appearance of a multi vane expander for exhaust waste heat recovery dates back to 1979 and was introduced by Robertson and Eckard [12]. As a preliminary phase, they built and tested multiple prototypes using several working fluids available at that time: output power ranged from 7 kW to 22 kW while inlet temperatures reached up to 340 °C. Afterwards, they proposed a conceptual design of an ORC system with multi vane expanders using the exhaust gases of a Mack Truck 676 Diesel Engine as the upper thermal source and claiming a recovery potential from 10% to 14% with reference to Fluorinol-50 at 17 bar and 315 °C. Subsequently, Badr et al. pointed out the benefits related to the intrinsic features of sliding vane expanders for ORC applications with respect to turbomachines and other positive displacement technologies: simple construction, compactness, lightweight, little maintenance, low noise and vibration, self-starting capabilities as well as tolerance to a wide range of vapor qualities [13,14]. Furthermore, they carried out a comprehensive modelling activity that became the baseline for most of the theoretical studies dealing with any kind of sliding vane machine [15,16]. As expander performance improvements, they outlined the need for a proper working fluid selection and a particular care for inlet port positioning, leakages, friction and heat transfer losses. The optimal port positioning was further investigated in [17] with reference to an air vane expander while in [18], using a semi-empirical model of a rotary vane expander, the Authors pointed out that the delayed closure of the working chambers can largely affect the filling factor. To reduce leakages, multiple design configurations have been proposed; in particular, in [19], the blades of a CO_2 expander, used to replace the expansion valve in a refrigeration system, were pushed outwards through springs in the rotor slots while in [20] the same goal was achieved through an injection of high pressure gas.

In recent years, a remarkable contribution to the investigation of sliding vane machines has been provided by the Authors through modelling, experimental [21] and numerical research works [22]. In [23], an experimental campaign on a small-scale ORC expander was carried out using the lubricant of an air compressor as the hot source and resulted in power recovery up to 1.7 kW and ORC efficiency up to 7.7% using R236fa as working fluid. This dataset was further used to validate the numerical CFD simulations on the machine that were performed thanks to a customized grid generation methodology [24,25] alternative to the one proposed in [26] for the study of a dual stage sliding vane expander for ORC automotive applications operating with R245fa. Later experimental works on larger and more advanced sliding vane expander prototypes were carried out still for low temperature applications and using R236fa; in particular, mechanical power recovery up to 3.2 kW and 3.7 kW and mechanical efficiency equal to 71.8% and 81.5% were achieved with respect to a simple and a regenerative ORC plant layouts [27].

Other research groups active in the sliding vane field have been looking at multi-vane expanders in domestic combined heat and power systems using ORC. In particular, numerical and experimental investigations were carried out on a four vane machine operating with R123 and at manometric pressure ratios between 1.54 and 4.33. Unlike the previous research groups, the experimental campaign was herein carried out at different revolution speeds and resulted in isentropic efficiencies in the range 17.2–58.3% [28]. On the other hand, a vane expander for micro-ORC application fed by boiler and working with R141b was experimentally investigated in [29] and resulted in a power output of 185 W in the optimal operating point at 4100 RPM. Small-scale systems working with siloxanes and developed in [30] reported design isentropic efficiency of 40–58% and mechanical power output in the range of 1–8 kW.

From the analysis of the literature, it can be therefore concluded that positive displacement vane machines can be a promising technology in the ORC field. However, in order to gain competitive advantage, together with lower manufacturing complexity and number of components, suitable performance levels must be reached. Past and current research efforts have been trying to tackle this challenge aiming at a reduction of volumetric and friction losses as well as to increase power density. Nonetheless, in the waste heat to power conversion field, the most valuable performance figure is eventually the net power output that an expander is able to provide rather than solely its overall efficiency.

For these reasons, in the current work we propose a novel concept to enhance the capabilities of positive displacement expanders which aims at maximizing the power recovery: the idea is to use a hot fluid injection at suction conditions to supercharge the expander cells during the

closed volume expansion phase. The supercharging technique is firstly presented in conceptual terms. A numerical model of a small-scale sliding vane ORC expander without supercharging is then introduced and validated using an experimental dataset related to an automotive application. Subsequently, the supercharging line is implemented in the expander model, parameterized in terms of four geometrical quantities and benchmarked with the non supercharged configuration through a comparison in terms of angular cell pressure traces. A genetic algorithm is eventually employed to optimize the auxiliary intake line.

2. Operating principle

The operation of a positive displacement expander can be theoretically broken down in five phases that are repeated every cycle. With reference to Fig. 1a, one can identify the suction phase in which the working chamber is filled with working fluid at high enthalpy conditions (5–1), followed by a closed volume phase in which the increase of chamber volume leads the working fluid to expand (1–2). The work on the moving boundaries of the control volume results in the actual conversion of the flow enthalpy into useful torque at the shaft. Then, an intermediate phase (2–3) may occur depending on the cell pressure value at the end of the closed volume expansion phase (p_2) with respect to the pressure imposed by the equipment connected downstream of the expander (p_{out}), e.g. the condenser pressure in ORC and steam applications or the atmospheric one for air expanders. In particular, if $p_2 > p_{out}$ an under-expansion takes place while if $p_2 < p_{out}$ the over-expansion is followed by a compression process up to p_{out}. Afterwards, during the discharge (3–4), the emptying of the expander cell takes place and it is followed by a final angular step in which its volume goes back to initial conditions (4–5).

In theoretical terms, suction and discharge are isobaric processes while the closed volume ones are adiabatic transformations. On the other hand, over and under expansions, which do not occur if the expander is well designed ($p_2 = p_{out}$), are isochoric processes. The net work per cell and per cycle is the area of the indicator diagram, as reported in Eq. (1).

$$W = \oint pdV \tag{1}$$

With respect to this baseline configuration, the operating principle of the proposed supercharging technique relies upon an auxiliary suction phase that occurs during the conventional closed volume expansion. In particular, supercharging the working chambers through an additional amount working fluid at suction conditions allows the cell pressure to raise and, in turn, the power density of the machine to increase without major design changes. This can be seen from the area of the modified indicator diagram shown in Fig. 1b.

The concept of supercharging has been previously applied to internal combustion engines. In particular, centrifugal as well as screw [31] and roots blowers [32] technologies have been used and they are now being reconsidered for hybrid and downsized vehicles [33,34]. Compared to engine supercharging, the expander supercharging that we propose has two major differences. The additional amount of working fluid that the supercharging provides is in fact not supplied to the conventional intake line of the expander but through an auxiliary connection placed downstream the conventional one. Moreover, there is no need of an external device that would require a power input from either the expander shaft or elsewhere since the additional amount of working fluid is supplied through a greater load on the pump of the ORC circuit, which deals with a liquid medium.

The application prospects of this technique are multiple. Indeed, an auxiliary intake line could be potentially installed to any positive displacement expander regardless of the technology. However, those machines that are characterized by simpler geometries would be more suitable to accurately locate the supercharging port. The application potential ranges from air to steam expanders as well as in expanders for heat to power conversion based on Organic Rankine (ORC) or Trilateral Flash cycles (TFC). In particular, the more the density drop during the expansion, the more effective the supercharging will be.

3. Numerical model

The sliding vane expander modelling was carried out with reference to a one-dimensional methodology implemented in the commercial software GT-SUITE™ v2017 [35]. This approach is a tradeoff between computational cost and accuracy. In fact, the lumped parameter simplification for the flow field in the expander cells as well as through the clearance gaps reduces the modelling effort and potential but, at same time, allows for fast simulations that are also suitable for optimization studies. A thorough explanation of the modelling methodology is available in references [36,37]. Nonetheless, in this paragraph the fundamentals and all the parameters considered in the expander modelling are reported for future reproducibility of the results.

The modelling approach considers a transient one-dimensional formulation of the conservation equations at the inlet and outlet ducts. The expander cells and the intake and exhaust manifolds are treated as capacities of variable and fixed volume respectively while the leakage paths are modelled using isentropic nozzle relationships. As concerns the friction modelling, four main locations are taken into account. Between blade tip and stator as well as between blade sidewalls and rotor slots, both dry and viscous friction phenomena apply. Conversely, between rotor and end wall covers, and at the bearings dominant friction is the viscous one. Hence, except for the bearings, the above-mentioned friction locations are also characterized by leakage flows.

In the model block diagram reported in Fig. 2, the different leakage paths are highlighted through different colors. On the other hand, the black connections represent pressure signals between the cells and the shaft module for power calculations. Pressure and speed data are eventually transferred to the friction module to compute the mechanical losses. The geometrical features of machine are essential to set up the numerical model. These input data refer to the overall dimensions of the machine as well as to the angular positioning of intake and

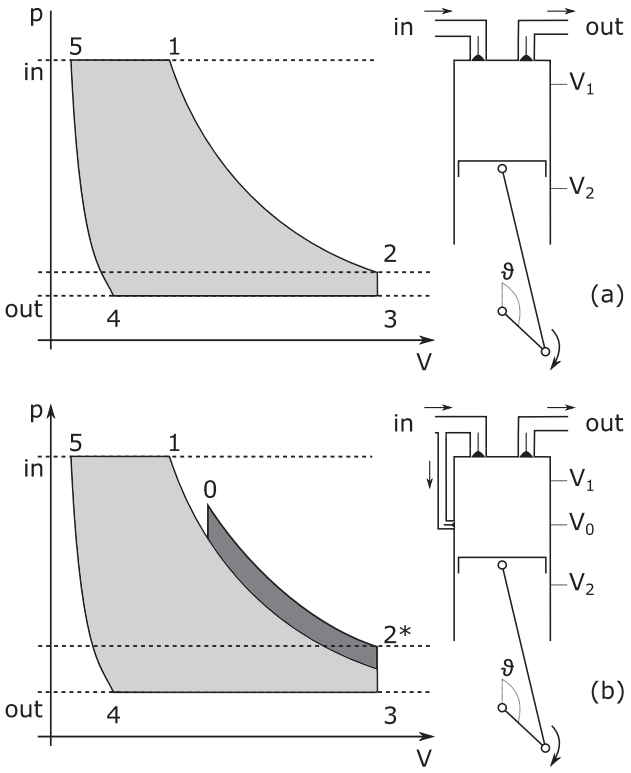

Fig. 1. Theoretical comparison of conventional (a) and supercharged (b) positive displacement expanders.

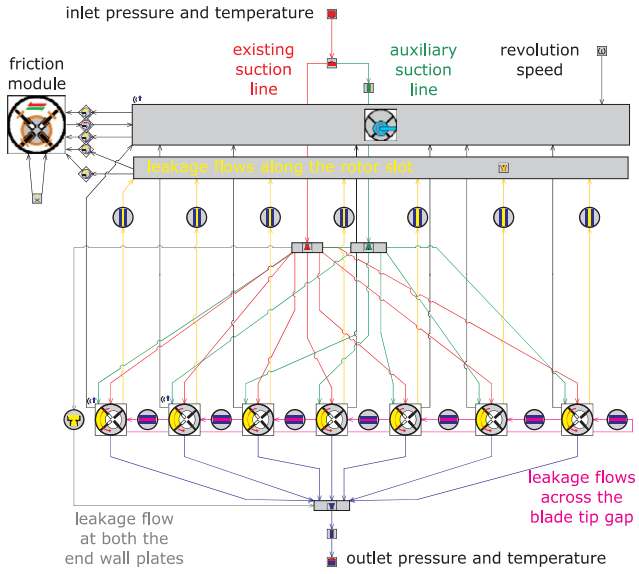

Fig. 2. Expander model block diagram (elaboration from [35]).

Table 1
Geometrical features of the sliding vane expander modelled and tested.

Number of cells	7
Rotor diameter	65.00 mm
Stator diameter	75.90 mm
Eccentricity	5.45 mm
Chamber width	60.00 mm
Blade thickness	3.96 mm
Blade length	17.00 mm

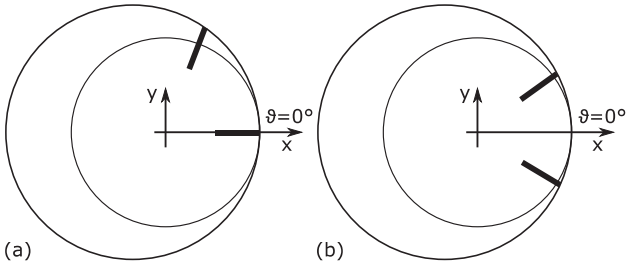

Fig. 3. Reference position in different angular coordinate systems: (a) literature, (b) GT-SUITE™.

Table 2
Details on angular port positioning.

	Literature (Fig. 3a)	GT-SUITE™ (Fig. 3b)
Intake port opening	4.4°	−18.3°
Intake port closing	48.0°	70.7°
Exhaust port opening	180.0°	157.3°
Exhaust port closing	320.0°	348.7°

Table 3
Equivalent orifice diameter (D_{eq}) of the leakage paths schematized in Fig. 2 and dry friction coefficient.

D_{eq} between rotor and housing (grey)	1.7 mm
D_{eq} between blade tip and stator (magenta)	1.5 μm
D_{eq} between blade side and slot (orange)	43 μm
Dry friction coefficient	0.1

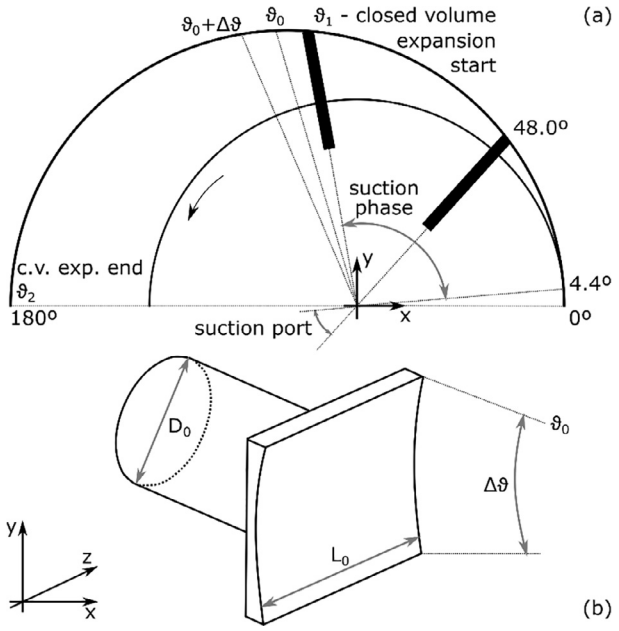

Fig. 4. Parameterization of the auxiliary intake line.

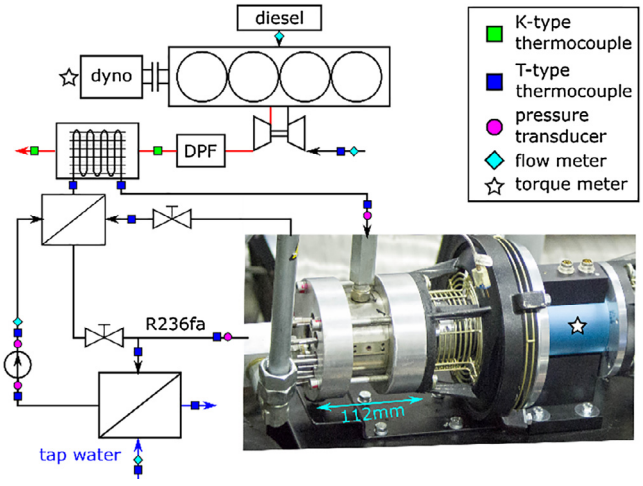

Fig. 5. Sensors layout and picture of the sliding vane expander.

exhaust ports. Details for the sliding vane expander herein investigated were retrieved from CAD measurements and are reported in Table 1.

With regards to the angular reference, it is worth to mention that most of the literature studies on vane machines consider as reference angular position the one in which one of the blades is completely inside the rotor slot, i.e. at the point in which rotor and stator are nearly tangent (Fig. 3a). On the other hand, for the implementation of the port positioning in the software platform, the reference angular position considers the bisecting line of the cell rather than the one of the blades (Fig. 3b). Hence, the angles are shifted of half vane width (25.7° in the current case). Table 2 reports a summary of the port positioning with reference to the two approaches. In particular, the expander is characterized by a radial intake port located on the stator and two axial discharge ports located on the end wall covers.

Besides the geometrical information, there are a series of input data that do not have a direct correspondence to the machine geometry or that are difficult to estimate from commonly available data, namely the equivalent diameters of the orifices that represent the leakage paths and the dry friction coefficient. These parameters were calibrated during the model validation by minimizing the root mean squared error (RMSE) between simulated and experimental values of mass flow rate

Table 4
Experimental campaign for model validation including measurements uncertainty.

Test (ESC point #)		A (7)	B (5)	C (9)	D (3)	E (11)	F (13)		
ICE	Torque	100	200	100	200	91	182	Nm	± 0.3%
	Speed	2175	2175	2750	2750	3325	3325	RPM	± 1
	Exhaust gas	0.063	0.08	0.073	0.1	0.077	0.114	kg/s	± 1%
	T exh. inlet	304.2	350.2	346.4	364.2	422.9	431.2	°C	± 0.4
	T exh. outlet	71.4	90.8	85.5	106.4	101.5	137	°C	± 0.4
ORC EXP	R236fa	0.101	0.139	0.127	0.179	0.167	0.208	kg/s	± 0.15%
	p inlet	9.0	12.5	11.6	16.5	16.0	21.0	bar	± 0.3
	p outlet	3.6	4.4	4.0	5.1	4.8	6.2	bar	± 0.3
	T inlet	72.7	89.0	84.8	101	100.1	119.5	°C	± 0.3
	T outlet	46.0	63.1	58.9	73.8	73.4	93.6	°C	± 0.3
	Torque	4.25	6.68	6.27	8.66	8.24	11.24	Nm	± 0.02
	Speed	1535	1569	1553	1573	1572	1606	RPM	± 1
	P_{exp}/P_{ICE}	3.1	2.4	3.5	2.4	4.4	3.0	%	
	η_{exp}	53.0	53.3	52.5	48.2	47.5	51.2	%	
	η_{ORC}	3.8	4.4	4.4	4.3	4.4	4.8	%	

Table 5
Testing procedure.

Start up	Water cooling loops for engine and ORC system turned on Engine at idle conditions in the dyno Pump at low speed to prevent organic fluid degradation due to overheating
Testing	Setup of the engine operating point in the dyno Pump speed increases Expander speed increases due to greater flow rate and pressure ratio Expander speed exceeds the synchronism speed of 15% Connection to the grid Pump speed manually adjusted until steady state conditions are reached
Shutdown	Engine at idle conditions in the dyno Expander speed decreases due to lower cycle pressure ratio Expander speed reaches the synchronism speed Pump speed gradually decreases Disconnection from the grid Pump at low speed until the ORC system is cooled down Shutdowns of Pump, Engine and Cooling loops

Table 6
Deviations between experimental and simulation results.

Test (ESC point #)	Mass flow rate	Torque
A (7)	4.7%	4.7%
B (5)	3.4%	2.4%
C (9)	2.2%	1.7%
D (3)	1.4%	0.6%
E (11)	4.7%	0.2%
F (13)	10.1%	0.9%
RMSE	5.2%	2.3%

and torque in the operating points discussed in Section 4. Final values are reported in Table 3.

The implementation of the supercharging technique in the expander simulation platform has been carried out through an auxiliary intake line in parallel with the existing one, i.e. fed by the same pressure and temperature boundary conditions. In the modelling scheme of Fig. 2, the existing intake line is reported in red while the auxiliary one is shown in green.

A supercharged sliding vane expander would be essentially characterized by an additional groove on the stator surface and an extra inlet pipe. Therefore, with reference to Fig. 4, the auxiliary intake line is fully defined by four parameters that are related to the angular position (ϑ_0), extension ($\Delta\vartheta$) and the axial length (L_0) of the auxiliary radial intake port, as well as by the diameter of the pipe which feeds the port (D_0). This latter parameter could also be representative of a valve opening.

Outlet pressure and temperature values, together with the expander speed, are the other boundary conditions. The numerical method considered is instead a 5th order explicit Runge-Kutta with a crank angle step of 0.5°. Average duration of a simulation using 1 logical processor of an Intel® Core™ i7-6700 CPU @ 3.40 GHz was 85 s while RAM usage was 500 MB.

4. Experimental validation

Prior to the implementation of the auxiliary intake line, the baseline sliding vane expander model, i.e. without supercharging, has been validated with respect to an experimental dataset. The measurement campaign refers to an automotive heat to power conversion application based on bottoming thermodynamic cycles. In particular, the expander was installed on an ORC system coupled with an IVECO F1C heavy-duty internal combustion engine, namely downstream its aftertreatment section. The ORC system was designed with reference to a usual operating point of the engine, namely 200 Nm at 2000 RPM [38]. Moreover, the ORC loop included a recuperator that allowed an increase of the heat recovery by pumping a greater amount of the organic working fluid (95% R236fa, 5% in mass of POE ISO VG 68 oil). R236fa was selected because of similar thermophysical properties to R245fa but at a much lower cost at the time of the experimental campaign. With regards to the phase of the working fluid during the experiments, R236fa was superheated throughout the expansion process, as it results from the measured pressure and temperature values at the inlet and the outlet of the machine. At the same time, experiments were carried out without exceeding the maximum threshold of 126.85 °C to prevent degradation of the organic fluid.

The sensors layout is shown in Fig. 5 together with a picture of the sliding vane expander [39]. A Coriolis flow meter was installed downstream the pump for direct mass flow rate measurement while pressure and temperature sensors were located across the machines and the heat exchangers. In particular, K-type thermocouples were used for the engine exhaust while T-type ones were installed in the refrigerant and cooling loops; this explains the different measurement uncertainty reported in Table 4. Direct measurement of the expander mechanical power was eventually performed through a torque meter also shown in Fig. 5. The experimental campaign was carried out with reference to six operating points of the European Stationary Cycle (ESC), a 13-mode, steady-state procedure for emission measurement from heavy-duty diesel engines [40]. The testing protocol including startup and shutdown sequences is reported in Table 5.

From the ORC system perspective, different mass flow rate and temperature of the heat source implied a change in the operating conditions of the recovery process. In turn, in the tests reported in Table 4, the expander operation changed in terms of pressure ratio and

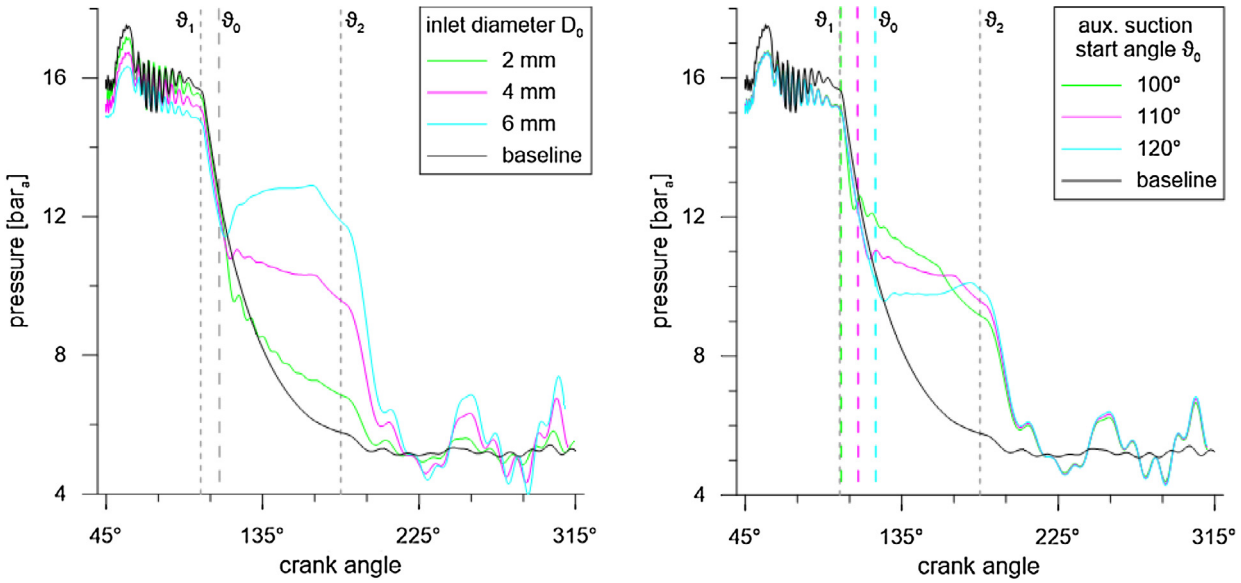

(a) inlet diameter of the auxiliary intake line (D_0)

(b) auxiliary intake start angle (ϑ_0)

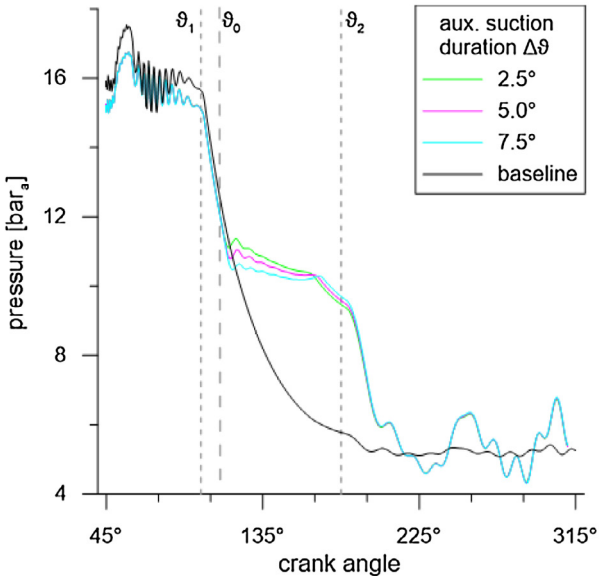

(c) auxiliary intake duration ($\Delta\vartheta$)

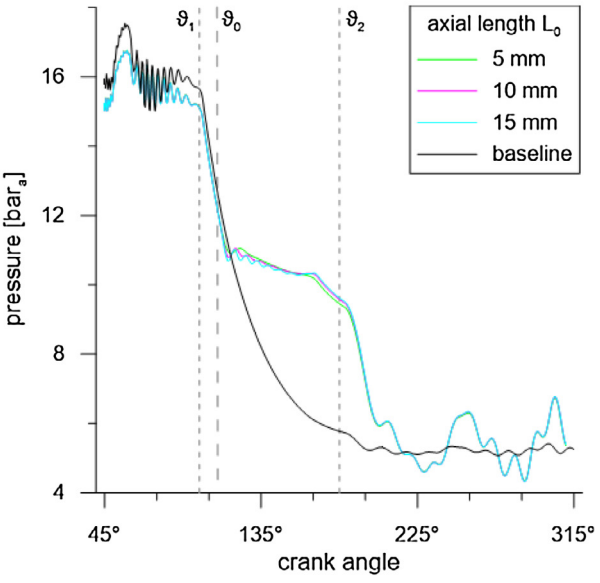

(d) axial length of the auxiliary intake port (L_0)

Fig. 6. Effects of the supercharging technique on the angular cell pressure evolution: baseline simulation refers to test D in Table 4 while reference values for the geometrical parameters are $D_0 = 4$ mm, $\vartheta_0 = 110^\circ$, $\Delta\vartheta = 5^\circ$, $L_0 = 10$ mm.

superheating but slightly with regards to the revolution speed since the machine was connected to a two-pole asynchronous electric motor that was used in generator mode.

With reference to Table 4, energy recovery increases at higher engine loads and revolution speeds due to greater exhaust gas mass flow rates and temperatures that are supplied to the bottoming ORC system. At 3225 RPM and 182 Nm, the sliding vane expander was able to provide up to 1.9 kW in mechanical form (3% of the engine power). Additionally, overall cycle efficiency reached 4.8%. Although the availability of the thermal waste decreased at low regimes, the recovery system was able to perform efficiently also at off-design conditions. At 3225 RPM and 91 Nm, mechanical power at the expander shaft reached 4.4% of the engine shaft power. In all the experiments, overall efficiency of the ORC power unit was always around 4.0%. As concerns the overall expander efficiency, computed as ratio between mechanical and isentropic powers, best performances of 53.3% occurred in the test case closest to the design point. At off-design conditions, characterized by higher heat gain, mechanical power recovered increased due to a higher working fluid mass flow rate and cycle pressure ratio. However, the large superheating in these operating points worsened the expander efficiency because of greater discharge pressures at the condenser.

Based on the experimental dataset presented in Table 4, the model validation resulted in the errors summarized in Table 6. Operating points at higher engine loads, which correspond to the highest expander revolution speeds and mechanical power outputs, show the lowest deviations from the experiments in terms of torque and mass flow rate of the organic fluid. Although the error on the flow rate can reach up to 10% and the one on the torque can get closer to 5%, the RMSE values are 5.2% and 2.3% respectively. Discrepancies between model and experiments are due to the number of assumptions made. Among them, the most restrictive one is having fixed the dimensions of the leakage paths regardless of the angular location or the operating conditions. In

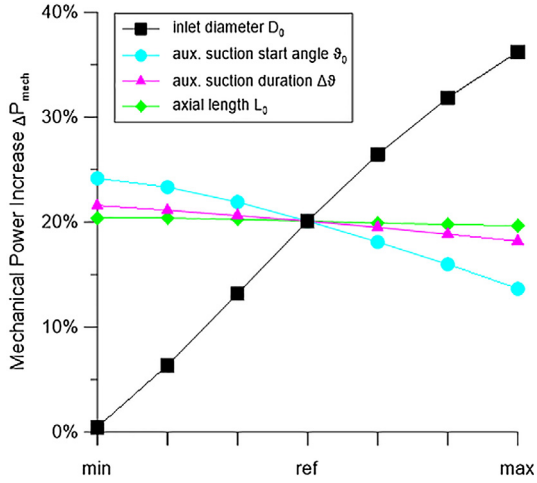

Fig. 7. Effects of different supercharging layouts on the expander mechanical power: reference value is test case D in Table 4 (1.40 kW).

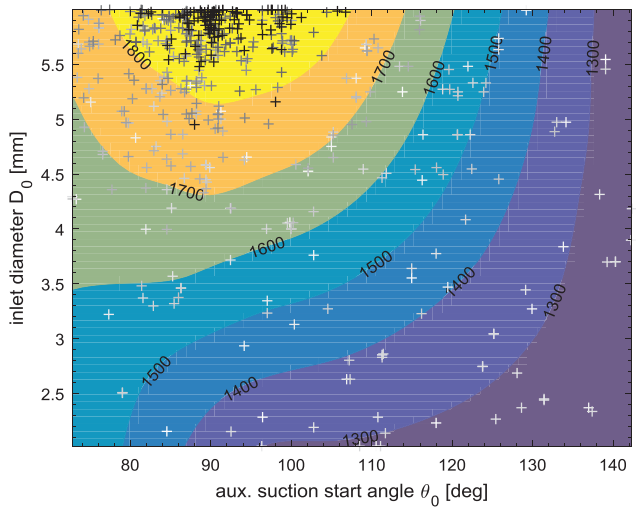

Fig. 8. Contours of optimization function with transition towards the optimized geometrical parameters: simulation points belonging to first generations are shown in white, last ones in black.

Table 7
Summary of optimized power recovery with the optimal supercharged configuration (D_0 6 mm, ϑ_0 91.5°, $\Delta\vartheta$ = 5°, L_0 = 10 mm).

Test	Mechanical power [W]		Gain
	Experimental	Supercharged	
A	683	1160	69.8%
B	1098	1700	54.9%
C	1020	1630	59.9%
D	1427	2040	43.0%
E	1356	2050	51.1%
F	1890	2720	43.9%
Avg.			50.6%

fact, actual clearance gaps depend on thermal expansion phenomena as well as dynamic ones. As shown in [21,22], the minimum thickness of the liquid film between blade tip and stator results from the forces applied to the rotor blades, which in turn depend on revolution speed, pressure ratio and angular position of the blade.

5. Results and discussion

5.1. Sensitivity analysis

The effects of the supercharging with regards to the four parameters shown in Fig. 4 were assessed with reference to the test D of the experimental campaign in Table 4, i.e. the one with the lowest discrepancy between measured and simulated performance (Table 6). In this first set of simulations shown in Fig. 6, boundary conditions were experimental the ones. The simulated angular pressure traces, however, do not refer to calculations at constant mass flow rate because of the different geometrical layouts of the auxiliary intake line.

In each subfigure, the results in Fig. 6 consider the variation of only one of the four geometrical parameters that define the supercharging line. For instance, in Fig. 6a the inlet diameter D_0 is varied from 2 mm to 6 mm while ϑ_0, $\Delta\vartheta$ and L_0 were kept at 110°, 5° and 10 mm respectively. On the other hand, in Fig. 6b, D_0 is kept at 4 mm while ϑ_0 is varied from 100° to 120°. The vertical dashed lines refer to the start and the end of the closed volume expansion phase which takes place between the angles ϑ_1 equal to 99.4° and ϑ_2 equal to 180°, as per Table 2; the auxiliary intake start angle ϑ_0 is further reported with a longer dashed line style.

Prior to the start of the closed volume expansion phase at 99.4°, a lower pressure can be noticed during the primary suction process due to the mass flow rate distribution between the primary and auxiliary intake lines. In fact, as shown in Fig. 6a, the smaller is the diameter of the auxiliary intake line the more this effect is reduced since the working fluid tends to go more favorably towards the primary intake line.

During the first part of the closed volume expansion phase, the pressure in the expander cell decreases as an adiabatic transformation since heat transfer phenomena between the expander and the environment were neglected in the modelling. Later on, the injection of different quantities of hot fluid inside the expansion cell leads to a deviation from the baseline angular pressure trace. In particular, with a pipe diameter D_0 of 6 mm, the sudden pressure rise outlined in Fig. 1 can be noticed and it stays until the end of the closed volume expansion (ϑ_2). The higher cell pressure at the beginning of the discharge in turn leads to an under-expansion and triggers pressure pulsations at the discharge. The amplitude of these oscillations is proportional to the mismatching between cell pressure at ϑ_2 and the condenser pressure; indeed, for smaller supercharging pipe diameters these phenomena are less noticeable.

During the discharge process, whose angular duration does not change since the supercharging does not affect the angular positioning of the exhaust port, the cell pressure depends on the machine geometry as well as on the volume of the outlet manifold which collects the different flow contributions from the emptying expander cells before delivering them to the outlet pipe. For instance, the crest-to-crest measurement of the two waveforms during the discharge provide an angular wavelength of approximately 50°, which essentially relates to the number of vanes of the machine (360°/7). Either way, these under (or over) expansion phenomena must be taken into account in the structural design of a supercharged expander. In fact, above all, the pressure peak at the beginning of the discharge results in a torque peak at the shaft which affects the overall shaft loading spectrum and possibly the machine lifetime.

Another remarkable effect, reported in Fig. 6b, is the angular positioning of the auxiliary intake line. An earlier start of the supercharging leads to an anticipated perturbation of the cell pressure whose effects consequently have a greater impact on the overall indicated power. Nonetheless, for the same injection duration, an anticipated positioning of the auxiliary intake port leads to a lower amount of working fluid injected in the cell due to a lower pressure difference between the cell pressure and the one upstream the expander. Conversely, if the injection of hot fluid is delayed, the supercharging is more effective and allows the compensation of the pressure decrease during the expansion.

This fact explains why, in the case of earlier supercharging, the cell pressure at the beginning of the discharge is lower. For instance, when the auxiliary suction starts at 100°, the pressure at ϑ_2 is equal to 9 bar, while if ϑ_0 equals to 120°, this value becomes 10 bar. The 1 bar discrepancy, however, is too little to severely affect the pressure pulsations during the discharge.

Due to the one-dimensional formulation of the model, the mass flow rate through the auxiliary intake port is fully defined by the pipe diameter D_0 and the pressure difference between suction conditions and the cell pressure at ϑ_0. In the range investigated and reported in Fig. 6c, the relative influence of the different injection durations on the angular pressure profile is minimal while the one related to the axial length L_0 is hardly noticeable in Fig. 6d.

Within the ranges considered in Fig. 6, a larger number of simulations was performed and presented in non-dimensional scale in Fig. 7. In particular, the chart compares the mechanical power increase of the supercharged cases with respect to the experimental baseline (test D in Table 4) of 1.40 kW. Each curve represents the variation of one geometrical parameter with respect to a reference configuration characterized by $D_0 = 4$ mm, $\vartheta_0 = 110°$, $\Delta\vartheta = 5°$, $L_0 = 10$ mm in which the mechanical power gain resulted around the 20% (1.68 kW). For instance, reducing the inlet pipe diameter in the auxiliary intake line up to the minimum value (2 mm) does not lead to any mechanical power benefit.

5.2. Optimized supercharged configuration

The sensitivity analysis reported in Section 5.1 showed that the geometrical parameters of the auxiliary intake port that mostly influence the expander mechanical power gain are the diameter of the inlet pipe D_0 and the angular positioning of the auxiliary port ϑ_0. This preliminary study further allowed the reduction of the number of variables to be optimized through a NSGA-III genetic algorithm [41] with population size equal to 50 and with reference to 10 generations. The optimization function aimed at maximizing the mechanical power in the six experimental operating points. The mathematical formulation reported in Eq. (2) considers the same weighting w_k for the dependent variables Y_k, i.e. the expander mechanical power in the six experimental operating conditions. Hence, $f(D_0,\vartheta_0)$ is the average mechanical power.

$$f(D_0,\vartheta_0) = \sum_{k=1}^{N} w_k Y_k \Big/ \sum_{k=1}^{N} w_k = \frac{1}{6}\sum_{k=A}^{F} P_{mech,k}(D_0,\vartheta_0) \tag{2}$$

Fig. 8 reports a summary of the optimization process within the simulation range considered for the independent variables D_0 and ϑ_0. In particular, the contours of the optimization function range from 1300 W to 1800 W and tend to increase at higher values of inlet pipe diameter of the supercharging port D_0 as well as earlier starts of the auxiliary intake ϑ_0, in agreement to what has been presented in Section 5.1. The chart additionally reports the transition from the first generations of simulations to the last, optimal, ones with grayscale color map. The optimal pair of D_0 and ϑ_0 values is 6 mm and 91.5° respectively; with reference to this optimized configuration an overall increase of mechanical power in all the experimental conditions reported in Table 4 was achieved. The results shown in Table 7 report an average mechanical power gain of 50.6%.

6. Conclusions

In this paper, a novel concept to enhance the recovery capabilities of positive displacement expanders has been presented and investigated through multiple methodological approaches. The idea behind the supercharging technique is to inject fluid at suction conditions during the closed volume expansion process such that the drop in cell pressure due to the expansion is compensated by the additional mass of high enthalpy working fluid. This technique is potentially applicable to any positive displacement expander technology.

The supercharging concept has been firstly theoretically introduced and then further exploited through a one-dimensional modelling of a sliding vane expander for ORC systems. Prior to the implementation of the auxiliary intake line, the modelling platform has been validated with reference to a small-scale sliding vane expander. In particular, the validation was carried out with respect to tests on an automotive ORC application at steady operating conditions in which the expander mechanical power ranged from 0.7 to 1.9 kW while its total efficiency ranged from 47.5% to 53.3%.

The supercharging line was parameterized in terms of four geometrical quantities and the effects on the angular cell pressure evolution and mechanical power gain investigated through a first set of simulations. From this sensitivity analysis it resulted that, for given suction conditions and expander revolution speed, the mechanical power increase due to the supercharging mostly depends on the start angle at which the auxiliary suction takes place as well as on the diameter of the inlet pipe of the supercharging intake line. An optimization study based on a non-dominated sorting genetic algorithm eventually allowed identifying optimal values for these geometrical quantities, namely 91.5° and 6 mm. This optimal configuration led to an average mechanical power gain with respect to the experimental performance of 50.6%.

Future developments of the research activity will aim at an experimental investigation of the supercharged technique to deeply understand potential and limitations of the approach.

Acknowledgements

The Authors are highly grateful to Dr. Giulio Contaldi and Dr. Stefano Murgia of Ing. Enea Mattei S.p.A. for their financial and technical support throughout this research activity. The contribution to the study of Mr. Marco Patrignani performed during his MSc thesis is further acknowledged.

The manuscript reports all the relevant data to support the understanding of the results. More detailed information and data, if required, can be obtained by contacting the corresponding author of the paper.

References

[1] M. Karvonen, R. Kapoor, A. Uusitalo, V. Ojanen, Technology competition in the internal combustion engine waste heat recovery: a patent landscape analysis, J. Clean. Prod. 112 (2016) 3735–3743, http://dx.doi.org/10.1016/j.jclepro.2015.06.031.
[2] S. Lion, C.N. Michos, I. Vlaskos, C. Rouaud, R. Taccani, A review of waste heat recovery and Organic Rankine Cycles (ORC) in on-off highway vehicle Heavy Duty Diesel Engine applications, Renew. Sustain. Energy Rev. 79 (2017) 691–708, http://dx.doi.org/10.1016/J.RSER.2017.05.082.
[3] T. Tartière, A world overview of the organic rankine cycle market, Energy Proc. 129 (2017) 2–9, http://dx.doi.org/10.1016/J.EGYPRO.2017.09.159.
[4] M. Usman, M. Imran, Y. Yang, B.-S. Park, Impact of organic Rankine cycle system installation on light duty vehicle considering both positive and negative aspects, Energy Convers. Manag. 112 (2016) 382–394, http://dx.doi.org/10.1016/J.ENCONMAN.2016.01.044.
[5] D. Di Battista, M. Di Bartolomeo, C. Villante, R. Cipollone, On the limiting factors of the waste heat recovery via ORC-based power units for on-the-road transportation sector, Energy Convers. Manag. 155 (2018) 68–77, http://dx.doi.org/10.1016/J.ENCONMAN.2017.10.091.
[6] D. Di Battista, M. Mauriello, R. Cipollone, Waste heat recovery of an ORC-based power unit in a turbocharged diesel engine propelling a light duty vehicle, Appl. Energy. 152 (2015) 109–120, http://dx.doi.org/10.1016/j.apenergy.2015.04.088.
[7] J. Peralez, P. Tona, O. Lepreux, A. Sciarretta, L. Voise, P. Dufour, M. Nadri, Improving the control performance of an Organic Rankine Cycle system for waste heat recovery from a heavy-duty diesel engine using a model-based approach, in: 52nd IEEE Conf. Decis. Control, 2013, pp. 6830–6836. http://doi.org/10.1109/CDC.2013.6760971.
[8] J. Treutler, T. Toepfer, O. Dingel, Combination of ORC system and electrified auxiliaries on a long haul truck equipped with 48-Volt board net, Energy Proc. 129 (2017) 778–785, http://dx.doi.org/10.1016/J.EGYPRO.2017.09.135.
[9] F. Pantano, R. Capata, Expander selection for an on board ORC energy recovery system, Energy 141 (2017) 1084–1096, http://dx.doi.org/10.1016/J.ENERGY.2017.09.142.
[10] M. Imran, M. Usman, B.-S. Park, D.-H. Lee, Volumetric expanders for low grade heat

and waste heat recovery applications, Renew. Sustain. Energy Rev. 57 (2016) 1090–1109, http://dx.doi.org/10.1016/J.RSER.2015.12.139.
[11] A. Kovacevic, Private communication, in: 3rd Short Course Forum Comput. Fluid Dyn. Rotary Posit. Displac. Mach., 2017. https://www.city.ac.uk/compressorsconference/short-course-on-compressors.
[12] C.S. Robertson, S.E. Eckard, A multi-vane expander, by adding power, can improve the fuel economy of long-haul diesel trucks, 1978. http://doi.org/10.4271/780689.
[13] O. Badr, P.W. O'Callaghan, M. Hussein, S.D. Probert, Multi-vane expanders as prime movers for low-grade energy organic Rankine-cycle engines, Appl. Energy (1984), http://dx.doi.org/10.1016/0306-2619(84)90060-6.
[14] O. Badr, S.D. Probert, P. O'Callaghan, Performances of multi-vane expanders, Appl. Energy 20 (1985) 207–234, http://dx.doi.org/10.1016/0306-2619(85)90024-8.
[15] O. Badr, P.W. O'Callaghan, S.D. Probert, Multi-vane expanders: geometry and vane kinematics, Appl. Energy 19 (1985) 159–182, http://dx.doi.org/10.1016/0306-2619(85)90006-6.
[16] O. Badr, S.D. Probert, P. O'Callaghan, Multi-vane expanders: vane dynamics and friction losses, Appl. Energy 20 (1985) 253–285, http://dx.doi.org/10.1016/0306-2619(85)90018-2.
[17] B.R. Singh, O. Singh, Analytical investigations on different air injection angles to optimize power output of a vaned-type air turbine, Proc. Inst. Mech. Eng. Part A J. Power Energy 224 (2009) 305–312, http://dx.doi.org/10.1243/09576509JPE837.
[18] V. Vodicka, V. Novotny, J. Mascuch, M. Kolovratnik, Impact of major leakages on characteristics of a rotary vane expander for ORC, Energy Proc. 129 (2017) 387–394, http://dx.doi.org/10.1016/J.EGYPRO.2017.09.249.
[19] B. Yang, X. Peng, Z. He, B. Guo, Z. Xing, Experimental investigation on the internal working process of a CO2 rotary vane expander, Appl. Therm. Eng. 29 (2009) 2289–2296, http://dx.doi.org/10.1016/J.APPLTHERMALENG.2008.11.023.
[20] X. Jia, B. Zhang, L. Pu, B. Guo, X. Peng, Improved rotary vane expander for trans-critical CO2 cycle by introducing high-pressure gas into the vane slots, Int. J. Refrig. 34 (2011) 732–741, http://dx.doi.org/10.1016/J.IJREFRIG.2010.12.005.
[21] G. Bianchi, R. Cipollone, Friction power modeling and measurements in sliding vane rotary compressors, Appl. Therm. Eng. 84 (2015), http://dx.doi.org/10.1016/j.applthermaleng.2015.01.080.
[22] G. Bianchi, R. Cipollone, Theoretical modeling and experimental investigations for the improvement of the mechanical efficiency in sliding vane rotary compressors, Appl. Energy 142 (2015), http://dx.doi.org/10.1016/j.apenergy.2014.12.055.
[23] R. Cipollone, G. Contaldi, G. Bianchi, S. Murgia, Energy recovery using sliding vane rotary expanders, Inst. Mech. Eng. - 8th Int. Conf. Compressors Their Syst. 2013, pp. 183–194, , http://dx.doi.org/10.1533/9781782421702.3.183 ISBN: 978-1-78242-169-6.
[24] G. Bianchi, S. Rane, A. Kovacevic, R. Cipollone, Deforming grid generation for numerical simulations of fluid dynamics in sliding vane rotary machines, Adv. Eng. Softw. (2016), http://dx.doi.org/10.1016/j.advengsoft.2017.05.010.
[25] G. Bianchi, S. Rane, A. Kovacevic, R. Cipollone, S. Murgia, G. Contaldi, Numerical CFD simulations on a small-scale ORC expander using a customized grid generation methodology, Energy Proc. (2017), http://dx.doi.org/10.1016/j.egypro.2017.09.199.
[26] G. Montenegro, A. Della Torre, M. Fiocco, A. Onorati, C. Benatzky, G. Schlager, Evaluating the performance of a rotary vane expander for small scale organic rankine cycles using CFD tools, Energy Proc. 45 (2014) 1136–1145, http://dx.doi.org/10.1016/J.EGYPRO.2014.01.119.
[27] S. Murgia, G. Valenti, D. Colletta, I. Costanzo, G. Contaldi, Experimental investigation into an ORC-based low-grade energy recovery system equipped with sliding-vane expander using hot oil from an air compressor as thermal source, Energy Proc. 129 (2017) 339–346, http://dx.doi.org/10.1016/J.EGYPRO.2017.09.204.
[28] P. Kolasiński, P. Błasiak, J. Rak, Experimental investigation on multi-vane expander operating conditions in domestic CHP ORC system, Energy Proc. (2017) 323–330, http://dx.doi.org/10.1016/j.egypro.2017.09.201.
[29] W. Suankramdee, T. Thongtip, S. Aphornratana, Development of a sliding vane expander in a micro-scale ORC system for utilizing low-grade heat, Energy Proc. 138 (2017) 817–822, http://dx.doi.org/10.1016/J.EGYPRO.2017.10.078.
[30] J. Mascuch, V. Novotny, V. Vodicka, Z. Zeleny, Towards development of 1–10 kW pilot ORC units operating with hexamethyldisiloxane and using rotary vane expander, Energy Proc. 129 (2017) 826–833, http://dx.doi.org/10.1016/J.EGYPRO.2017.09.196.
[31] R. Wade, S. Murphy, P. Cross, C. Hansen, A Variable Displacement Supercharger Performance Evaluation, in: WCX™ 17 SAE World Congr. Exp., SAE International, 2017. http://dx.doi.org/https://doi.org/10.4271/2017-01-0640.
[32] S. Pradhan, P.K. Jeemon, Modeling and Validation of Roots type Supercharger using GT-Suite, in: WCX SAE World Congr. Exp., SAE International, 2018.
[33] B. Hu, J.W.G. Turner, S. Akehurst, C. Brace, C. Copeland, Observations on and potential trends for mechanically supercharging a downsized passenger car engine: a review, Proc. Inst. Mech. Eng. Part D J. Automob. Eng. 231 (2016) 435–456, http://dx.doi.org/10.1177/0954407016636971.
[34] H.H. Tran, B. Richard, K. Gray, J.M. Hall, Developing a performance specification for an electric supercharger to satisfy a range of downsized gasoline engine applications, in: SAE 2016 World Congr. Exhib., SAE International, 2016. https://doi.org/10.4271/2016-01-1041.
[35] Gamma Technologies, GT-SUITE Flow Theory Manual, 2017.
[36] G. Bianchi, F. Fatigati, S. Murgia, R. Cipollone, Design and analysis of a sliding vane pump for waste heat to power conversion systems using organic fluids, Appl. Therm. Eng. 124 (2017), http://dx.doi.org/10.1016/j.applthermaleng.2017.06.083.
[37] G. Bianchi, S. Kennedy, O. Zaher, S.A. Tassou, J. Miller, H. Jouhara, Numerical modeling of a two-phase twin-screw expander for Trilateral Flash Cycle applications, Int. J. Refrig. 88 (2018) 248–259, http://dx.doi.org/10.1016/J.IJREFRIG.2018.02.001.
[38] R. Cipollone, G. Bianchi, A. Gualtieri, D. Di Battista, M. Mauriello, F. Fatigati, Development of an Organic Rankine Cycle system for exhaust energy recovery in internal combustion engines, J. Phys. Conf. Ser. 655 (2015), http://dx.doi.org/10.1088/1742-6596/655/1/012015.
[39] G. Bianchi, Exhaust waste heat recovery in internal combustion engines, Libreria Universitaria Benedetti, IT, 2015. http://doi.org/10.13140/RG.2.1.4095.7282.
[40] E. Parliament, DIRECTIVE 1999/96/EC, 1999. http://eur-lex.europa.eu/legal-content/EN/TXT/?uri=CELEX%3A31999L0096.
[41] K. Deb, H. Jain, An evolutionary many-objective optimization algorithm using reference-point-based nondominated sorting approach, Part I: Solving problems with box constraints, IEEE Trans. Evol. Comput. 18 (2014) 577–601, http://dx.doi.org/10.1109/TEVC.2013.2281535.